High Speed Permanent Magnet Assisted Synchronous Reluctance Machines - Part I: A General Design Approach

Gianvito Gallicchio, Mauro Di Nardo, *Member, IEEE,* Marco Palmieri, *Member, IEEE,* Alessandro Marfoli, Michele Degano, *Senior Member, IEEE,* Chris Gerada, *Senior Member, IEEE,* and Francesco Cupertino, *Senior Member, IEEE*

***Abstract*—The design of synchronous reluctance machines with and without permanent magnets assistance constitutes a challenging engineering task due to the numerous design variables and performance indexes to be considered. The design complexity increases even further when the application requires high speed operation, with consequent rotor structural constraints and related effects on the electromagnetic performance. Structured as two-parts companion papers, this work proposes a comprehensive design procedure able to consider all the non-linear aspects of the machine behaviour, greatly reducing the number of independent design variables, without worsening the computational burden. In particular, the non linear behaviour of the rotor iron ribs and the effect of the permanent magnets on the structural design are all taken into account with the proposed iterative design procedure targeting the achievement of a desired power factor. The proposed method will be then used to draw some preliminary design considerations highlighting the several trade-offs involved in the design of high speed permanent magnet assisted synchronous reluctance machine. Part I is setting the theoretical bricks that will be further expanded and experimentally validated in the companion paper Part II.**

***Index Terms*—Analytical design, finite element analysis, high speed, iron ribs, permanent magnet, structural rotor design, synchronous reluctance machines.**

I. Introduction

Power factor, constant power speed range and torque density of synchronous reluctance machines (SyRM) can all be improved with the insertion of permanent magnets (PM) within the rotor structure [1], [2]. The design process of the resulting electrical machine (hereafter called permanent magnet assisted synchronous reluctance machine, PMaSyRM) is far from being standardized as it involves multiple design choices with conflicting results [3]. The design task becomes even more challenging when the application requires high speed operations due to the increased complexity added by the rotor structural design [4], [5].

Two main strategies have been proposed in recent years to design PMaSyRMs. The first one divides the design process into two or more steps [6] while the other approach treats the electrical machine as a unique device [7].

G. Gallicchio, M. Palmieri and F. Cupertino are with the Department of Electrical Engineering and Information Technology, Politecnico di Bari, Bari, 70126 Italy e-mail: gianvito.gallicchio@poliba.it.

M. Di Nardo, A. Marfoli, M. Degano and C. Gerada are with the Power Electronics and Machine Control Group, University of Nottingham, Nottingham, NG7 2GT, UK.

With the first design approach, both stator and rotor geometries are identified following the design rules of SyRMs, thus disregarding the effect of the permanent magnet assistance [8]. After this first stage, the effects of the PM insertion are evaluated with analytical or finite element tools. In particular, the PM quantity is dictated by the adopted design criterion, i.e. obtain either the widest constant power speed range or the maximum torque increment [9], [10] subject to the constraints imposed by the demagnetization phenomena [11]. The distribution of the PMs within the rotor flux barriers is instead selected so to reduce the harmonic content of the resulting airgap flux density and consequently the torque ripple. Also this design step can be carried out analytically, as elegantly reported in [12], or by finite element method [13], which has the advantage of including all the secondary phenomena within the analysis (e.g. localized rotor saturation and slot harmonics effects). When designing PMaSyRMs for high speed applications, a further mechanical design step must be considered to determine the iron rib dimensions and distribution required to guarantee the rotor structural integrity at the maximum speed [14].

On the contrary, the second design philosophy treats the PMaSyRM as a unique device thus the PM electromagnetic and structural effects are considered from the initial stage. This approach has been implemented either with the aid of a simplified equivalent magnetic circuit [7] or by brute force FE-based design optimization [15]. In the first case, the hypothesis of linearity of the magnetic materials and the fact that the cross-saturation effect is neglected represent the main drawbacks. On the contrary, the FE-design optimization approach is very accurate but computationally more expensive than the analytical one. Albeit its high accuracy, FE-based optimization of multi-objective problems with a very wide research space often leads to sub-optimal solutions depending on the given time frame [16]. Indeed, unless a powerful computational cluster is available, dividing the research space and so the design procedure into several steps could lead to better results [17].

Although the comprehensive analytical design approach presented in [11], [18] is effective, at least as preliminary design stage to be followed by a FE refinement, it does not consider the permanent magnet influence on the stator design and neglects the soft magnetic material non-linearity. An interesting attempt to consider part of the non linearity effect

has been proposed in [19] where the saturation of the main flux path (d-axis in Fig. 1) is considered with the aid of a non linear magnetic equivalent circuit. For high speed applications, when the dimensions of the rotor iron ribs become relevant, also the saturation of the high reluctance flux path (q-axis in Fig. 1) plays a major role in determining the machine performance. Indeed, the estimation of the q-axis inductance and of the PM flux linkage assuming a certain saturation level of the iron ribs looses accuracy as the speed increases, i.e. as the rib dimensions increase. Indeed, the PM insertion into the rotor flux barriers complicates both structural and electromagnetic aspects. In fact, the PM increases the rotor mass to be sustained by the iron ribs and the presence of the latter non-linearly affects the machine performance, i.e. PM flux linkage and q-axis inductance.

This work, structured as two-parts companion papers, extends the methodology presented in [20] in order to design PMaSyRMs suitable for high speed operations fully considering the effect of the PM presence and without neglecting the interaction between the structural targets of having iron ribs and their non linear electromagnetic behaviour. Indeed, the analytical performance prediction, used during the design, is enhanced by the calculation of the PM flux linkage and q-axis inductance with a non-linear lumped-parameters magnetic circuit capable of taking into account the saturation of the structural iron ribs leading to the correct sizing of the PMs which guarantee a specified performance requirement. The proposed design approach allows to define both stator and rotor geometries, which can be then FE-refined prior the manufacturing.

In the next section, the proposed analytical design procedure is described in depth. The following sections III and IV report the FE validation of a wide range of designs along with a methodology to further improve the performance calculation accuracy. Section V provides some preliminary design considerations related to the optimal machine selection.

In the second part of this work, the proposed design approach will be used to identify the optimal geometries and related performance that can be achieved with and without the PM assistance as function of the speed. The outlined design considerations will be then experimentally validated showing the test results of a 8.5kW-80krpm PMaSyR prototype.

II. Analytical design

In this section torque and power factor are expressed as functions of two per-unit variables: the split ratio sr and the magnetic ratio mr, defined as:

$$sr = \frac{r_r}{r_s}, \quad mr = \frac{B_g}{B_{fe}} \tag{1}$$

where r_r is the rotor radius, r_s the stator outer radius, B_g the amplitude of the first harmonic of the airgap flux density and B_{fe} the imposed iron flux density. The latter is the peak value of flux density within the stator yoke and it is chosen to be close to the knee point of the stator material BH curve, whereas the flux density in the stator tooth can be assumed to be equal to B_{fe} or, as in this work, 20% higher. The remaining geometrical parameters, all depicted in

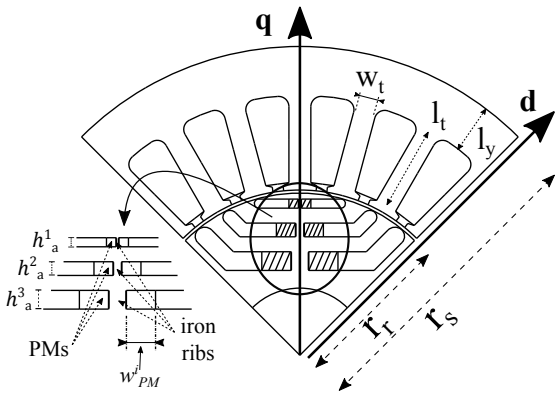

Fig. 1: Machine parametrization.

Fig. 1, will be expressed in terms of these two independent quantities, allowing to fully define the machine geometry for a given outer envelope (i.e. outer stator radius r_s and stack length L). In the next two subsections, first the main equations used to analytically estimate torque and power factor are recalled, then the non-linear q-axis equivalent magnetic circuit is described. The third subsection outlines different PM design criteria, while in the last part the iterative procedure required to calculate both PM flux linkage and q-axis inductance is described.

A. Main design equations

The torque produced by SyRMs or PMaSyRMs can be expressed, in its general form, as follows:

$$T = \frac{3}{2} \cdot p \cdot (\lambda_d \cdot i_q - \lambda_q \cdot i_d) \tag{2}$$

while the internal power factor, defined by the sine of the angular displacement between the current and flux linkage vectors (Fig. 2), can be written as:

$$ipf = \sin\left[\arctan\left(\frac{i_q}{i_d}\right) - \arctan\left(\frac{\lambda_q}{\lambda_d}\right)\right] \tag{3}$$

where p is the number of pole pairs, i_d and i_q are d-axis and q-axis currents, whereas λ_d and λ_q are d-axis and q-axis flux linkages.

For a given couple of independent design variables (sr, mr), the d-axis flux per pole is defined $(2 \cdot r_r \cdot L \cdot B_g/p)$, therefore

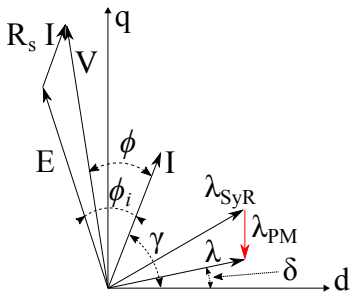

Fig. 2: Vector diagramm of PMaSyRMs.

the tooth width (w_t) and stator yoke radial thickness (l_y) can be evaluated imposing the iron flux density B_{fe} [21]:

$$l_y = \frac{r_s}{p} \cdot sr \cdot mr \tag{4}$$

$$w_t = \frac{\pi \cdot r_s}{3 \cdot q \cdot p} \cdot sr \cdot mr \tag{5}$$

where q is the number of slots per pole per phase. The stator tooth length (l_t) follows by simple geometrical considerations:

$$l_t = r_s \cdot \left[1 - sr \cdot (1 + \frac{\pi \cdot mr}{2 \cdot p})\right] - g \tag{6}$$

where g is the airgap thickness.

The complete rotor geometry, except for the PM dimensions, can be defined following the rules reported in [22]. On one hand, the barriers angular positions (in electrical degrees) at the airgap can be calculated so to obtain a uniform distribution of the equivalent rotor slots as in (7):

$$\Delta\alpha^i = \frac{2\pi}{n_r} \tag{7}$$

where n_r is the number of equivalent rotor slots whose choice depends on the number of stator slots if the minimum torque ripple condition is pursued. On the other hand, the i^{th} barrier height h_a^i and surface S_b^i are uniquely defined imposing barriers having the same permeance (eq. (8)) and the total iron thickness along the q-axis equal to the stator yoke thickness.

$$P_b = \frac{\mu_0 S_b^i}{h_a^i} = K \qquad \text{for} \quad \mathrm{i} = 1, 2, ..., n \tag{8}$$

Dealing with PMaSyRMs, if the PM height is imposed equal to the flux barrier one, the only remaining degree of freedom is the PM width w_{PM}. It is worth to underline that the above rotor design choices (which are just one option) allow minimizing the torque ripple [23]. Indeed, uniform distribution of the equivalent rotor slots and barriers with equal permeance allow obtaining a direct proportionality between the stator and rotor m.m.f. so to minimize their harmonic interaction, if the local saturation effects and the influence of different tangential ribs thicknesses are neglected.

The current components are calculated imposing the airgap flux density (B_g and so the magnetic ratio mr) and the cooling system. In fact, the d-axis current can be inferred according to the Ampère's law:

$$i_d = \frac{\pi}{3} \frac{k_c g}{\mu_0} \frac{p}{k_w N_s} B_g \tag{9}$$

where N_s is the number of turns in series per phase, k_w is the winding factor, μ_0 is the vacuum permeability and k_c is the Carter's coefficient.

Conversely, the q-axis current can be computed knowing the maximum current I_{max} which can be calculated imposing the cooling capability k_{cool} as in (10):

$$I_{max} = \frac{1}{3N_s} \sqrt{\frac{k_{fill} A_{slots}}{2\rho_{cu}(L + L_{ew})} (2\pi r_s L k_{cool})} \tag{10}$$

where k_{fill} is the chosen slot fill factor, k_{cool} is defined as the ratio between the allowed copper losses and the stator outer surface, ρ_{cu} the copper resistivity, while L_{ew} and A_{slot} are the end-winding length the slot area which both follow from geometrical considerations.

As just described, for a given split and magnetic ratio, it is possible to calculate the current components once the iron flux density B_{fe} and the cooling system k_{cool} are defined. In order to estimate both torque and power factor the flux linkages λ_d and λ_q need to be accurately calculated. The latter can be written as:

$$\lambda_d = (L_{dm} + L_s) i_d + L_{dq} i_q - \lambda_{PM-d} \tag{11}$$

$$\lambda_q = L_{dq} i_d + (L_{qm} + L_{q-rib} + L_s) i_q - \lambda_{PM-q} \tag{12}$$

where L_{dm} and L_{qm} are the d- and q-axis magnetizing inductances, L_{q-rib} takes into account the flux short-circuited via the structural iron ribs, L_{dq} accounts for the cross-coupling effects, L_s is the leakage inductance and λ_{PM-d} and λ_{PM-q} are the d- and q-axis fluxes produced by the PMs. Dealing with SyRMs, the last terms are clearly zero. Both L_{dq} and λ_{PM-d} terms are neglected in the analytical design because they can only be accurately estimated by means of FE analysis. On the contrary, many analytical formulations are available in literature to calculate all the components of the leakage inductance L_s [24]. Regarding the magnetizing component of the d-axis inductance, it can be easily calculated neglecting the iron saturation as:

$$L_{dm} = \frac{\pi}{2} \mu_0 k_w \left(\frac{N}{p}\right)^2 \frac{r_r L}{k_c g} \tag{13}$$

where k_w is the winding factor. These formulations ((9) and (13)) lead to an overestimation of the d-axis inductance while the d-axis current is underestimated. This limit can be overcome by introducing a factor ($k_{d-sat} > 1$) which takes into account the saturation of the d-axis magnetic flux path. The evaluation of k_{d-sat} is performed by solving a simplified equivalent magnetic circuit as proposed in [21].

A q-axis equivalent circuit accounting for the non linear behaviour of the iron ribs is presented in the next subsection. It is worth to underline that the stator and rotor geometrical parameters are calculated disregarding the permanent magnets flux. This is clearly valid for SyRM; however, when designing PMaSyRMs, this assumption remains valid as long as the PM flux linkage does not substantially affect the total flux. This detail will be discussed thoroughly in Section V.

B. Non-linear q-axis equivalent magnetic circuit

If only the q-axis component of the stator m.m.f. is considered, the rotor iron segments assume different magnetic potentials. In other words, the rotor magnetically reacts to the applied stator m.m.f.. The no-load flux linkage due to the PMs and the q-axis inductance can be calculated solving the equivalent magnetic circuit reported in Fig. 3a for a rotor with 3 barriers per pole. In the latter, the m.m.f generators F^1, F^2 and F^3 stand for the q-axis stator magneto-motive forces averaged along the periphery of the rotor with intervals equal to the rotor pitches $\Delta\alpha^i$ as shown in Fig. 4. The

reluctances related to the airgap paths can be calculated for the i$^{\text{th}}$ equivalent circuit branch as:

$$R_g^i = \frac{g}{\mu_0 \cdot \Delta\alpha^i \cdot r_r \cdot L} \tag{14}$$

The PMs are represented by the series of the m.m.f. generators U_m^i and the reluctances R_m^i which can be both calculated for the i$^{\text{th}}$ barrier as:

$$U_m^i = B_{rem} \cdot w_{PM}^i \cdot L \cdot R_m^i \tag{15}$$

$$R_m^i = \frac{h_{PM}^i}{\mu_{PM} \cdot \mu_0 \cdot w_{PM}^i \cdot L} \tag{16}$$

where B_{rem} is the residual flux density of PM material which is set to zero when designing SyRM and μ_{PM} is the relative permeability of the PM. The remaining part of the barrier is taken into account by the reluctances R_a^i equal to:

$$R_a^i = \frac{h_a^i}{\mu_0 \cdot w_a^i \cdot L} \tag{17}$$

being h_{PM}^i, h_a^i, w_{PM}^i, w_a^i the heights and the widths of i$^{\text{th}}$ PM and flux barrier, respectively. Although a different choice is possible, in this work the PM height h_{PM}^i is considered equal to the flux barrier one h_a^i.

The structural iron ribs are modeled with flux generators ϕ_r^i in parallel with the reluctances R_r^i which can be both calculated as:

$$\phi_r^i = B_{rib0}^i \cdot w_r^i \cdot L \tag{18}$$

$$R_r^i = \frac{h_r^i}{\mu_{rib-diff}^i \cdot \mu_0 \cdot w_r^i \cdot L} \tag{19}$$

where the radial height of the ribs h_r^i is here considered equal to the respective barrier one h_a^i while their thickness w_r^i follows from mechanical considerations.

Indeed, the iron rib thickness of the i^{th} barrier can be computed adopting a simplified analytical model which considers only the centrifugal force F_c^i acting on the relative flux guide and PM [25] as shown by the shaded region in Fig. 4b:

$$w_r^i = \frac{k_s}{\sigma_s L} \cdot F_c^i = \frac{k_s}{\sigma_s L} \cdot (m_{PM}^i + m_{fg}^i) \cdot R_{cg}^i \cdot \omega_m^2 \tag{20}$$

where k_s is a safety factor (usually between 2 and 3), σ_s is the yield strength of the rotor lamination, m_{fg}^i is the flux guide mass and m_{PM}^i the PM masses which have to be sustained by the i^{th} iron rib, R_{cg}^i is the coordinate of the center of mass of the considered region, and ω_m is the mechanical speed.

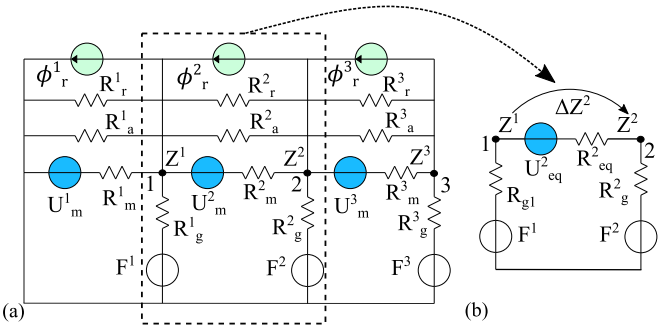

Fig. 3: a) q-axis magnetic equivalent circuit; b) Thévenin equivalent

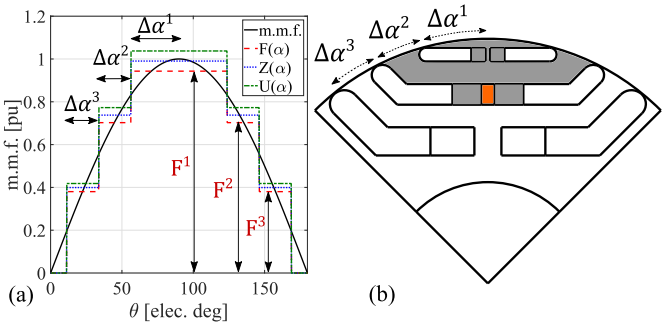

Fig. 4: a) stator q-axis m.m.f. b) rotor parametrization.

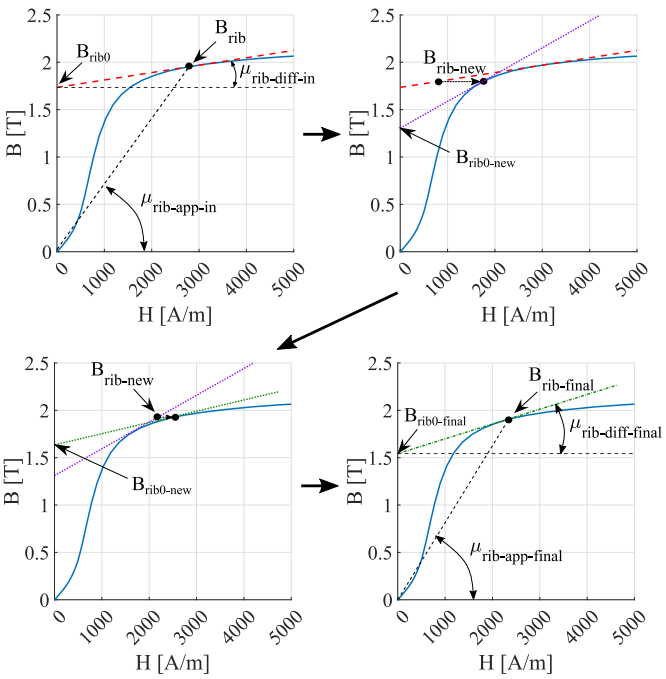

Fig. 5: Example of B_{rib0}, $\mu_{rib-diff}$ and $\mu_{rib-app}$ identification for the iron ribs modeling.

The iron rib permeability $\mu_{rib-diff}^i$ and the flux density B_{rib0}^i both depend on the rib working point B_{rib}^i on the non-linear B-H curve of the rotor soft magnetic material as depicted in Fig. 5. Indeed, they are defined by the line tangent to the point B_{rib}^i which can be expressed as:

$$B_{rib}^i = B_{rib0}^i + \mu_{rib-diff}^i \cdot H_{rib}^i \tag{21}$$

from which it is possible to calculate both ϕ_r^i and R_r^i required to solve the equivalent magnetic circuit.

It is a common practice to consider all the iron ribs equally saturated at a predefined value B_{rib} whatever operating condition is analyzed. This approximation is acceptable as long as the dimensions of the ribs are relatively small and the shunted flux does not substantially modify the machine performance. Clearly, this assumption looses its validity as the speed increases since the iron ribs dimensions become more important. In fact, as the speed increases the effective working point B_{rib}^i considerably deviates from the a-priori defined value; moreover each iron rib may assume different operating points. Consequently, an iterative procedure is required as the

speed increases in order to update the parameters defining the iron ribs behaviour, i.e. the flux generators ϕ_r^i and the reluctances R_r^i. Furthermore, when the PMaSyRM case is considered, these values are also affected by the amount of PM material placed within the rotor slots and their distribution.

C. PM design criteria

The q-axis equivalent magnetic circuit reported in Fig. 3a can be simplified applying the Thèvenin theorem; Fig. 3b shows the equivalent of one branch of the circuit, where R_{eq}^i is the parallel between R_a^i, R_m^i and R_r^i, while U_{eq}^i can be computed as:

$$U_{eq}^i = R_{eq}^i \cdot L \cdot [w_{PM}^i \cdot B_{rem} - w_r^i \cdot B_{rib0}^i] \tag{22}$$

Writing the first Kirchhoff's law at the nodes 1, 2 and 3 in Fig. 3 and expressing the flux flowing in the connected branches as a function of the m.m.f. related to the PM and ribs ($\mathbf{U_{eq}}$), stator excitation ($\Delta\mathbf{F}$) and rotor reaction ($\Delta\mathbf{Z}$), it is possible to write the following matrix equation:

$$\mathbf{A} \cdot \Delta\mathbf{Z} = \mathbf{B} \cdot \mathbf{U}_{eq} + \mathbf{C} \cdot \Delta\mathbf{F} \tag{23}$$

where $\mathbf{A}$, $\mathbf{B}$ and $\mathbf{C}$ are matrices defined by the barriers, airgap, magnets and ribs reluctances while the three vectors $\mathbf{U_{eq}}$, $\Delta\mathbf{Z}$ and $\Delta\mathbf{F}$ are defined as follows:

$$\mathbf{U}_{eq} = \begin{bmatrix} U_{eq}^1 \\ U_{eq}^2 \\ U_{eq}^3 \end{bmatrix}, \Delta\mathbf{F} = \begin{bmatrix} F^1 \\ F^2 - F^1 \\ F^3 - F^2 \end{bmatrix}, \Delta\mathbf{Z} = \begin{bmatrix} Z^1 \\ Z^2 - Z^1 \\ Z^3 - Z^2 \end{bmatrix} \tag{24}$$

As shown in eq. (22), U_{eq}^i depends on the PM widths which have to be identified according to a specific criterion. One possible option is to design the PM dimensions in order to maximize the flux weakening capability of the machine and so its constant power speed range. It is well known that this condition is achieved when the PM flux linkage equals the q-axis flux at the rated condition [26]:

$$\lambda_{PM-NC} = L_q I_n \tag{25}$$

where λ_{PM-NC} is the desired PM flux linkage and L_q is the total q-axis inductance (sum of the magnetizing and leakage components). An elegant way to implement this PM design criterion, also known as natural compensation ($_{NC}$), is to impose the fluxes entering the branches of the stator m.m.f generators (reported in Fig. 3a with the symbol F^i) equal to zero. In other words, the rotor magnetic potentials (Z_i) have to equal the stator ones (F_i). Imposing the condition $\Delta\mathbf{Z} = \Delta\mathbf{F}$ allows to determine the equivalent m.m.f. $\mathbf{U_{eq}}$:

$$\mathbf{U}_{eq} = \mathbf{B^{-1}} \cdot (\mathbf{A} - \mathbf{C}) \cdot \Delta\mathbf{F} \tag{26}$$

from which the PM widths w_{PM-NC}^i can be calculated:

$$w_{PM-NC}^i = \frac{1}{B_{rem}} \left[\frac{U_{eq}^i}{R_{eq}^i \cdot L} + w_r^i \cdot B_{rib0}^i \right] \tag{27}$$

supposing a certain iron rib dimension w_r^i and electromagnetic exploitation B_{rib}^i.

It is worth to underline that adopting this PM sizing approach along with the criterion of designing the rotor flux barriers with equal permeance, allows minimizing also the torque ripple. In fact, when these two criteria are adopted, the matrix $\mathbf{B^{-1}} \cdot (\mathbf{A} - \mathbf{C})$ is diagonal, which means that the equivalent PM m.m.f. ($U_{eq}(\alpha)$ in Fig. 4) is proportional to the stator m.m.f $F(\alpha)$. Therefore the harmonic interaction between these two m.m.f. is minimized.

For this reason, if another PM design method is adopted, it is convenient to simply scale the PM dimension obtained with the natural compensation criterion (w_{PM-NC}) in order to keep the proportionality between stator and PM m.m.f. For example, if a certain value of internal power factor is desired (ipf^*), the required PM flux linkage λ_{PM-q}^*, neglecting both cross coupling terms (L_{dq} and λ_{PM-d}), would be:

$$\lambda_{PM-q}^* = L_q i_q - \lambda_d \left\{ \tan \left[\arctan \left(\frac{i_q}{i_d} \right) - \arcsin \left(ipf^* \right) \right] \right\} \tag{28}$$

Once the PM flux linkages are known in the natural compensation condition λ_{PM-NC} and in the condition providing a given internal power factor λ_{PM-q}^*, the new PM dimensions can be simply calculated as:

$$\mathbf{w}_{PM}^* = \mathbf{w}_{PM-NC} \frac{\lambda_{PM-q}^*}{\lambda_{PM-NC}} \tag{29}$$

Once the PMs widths are defined, the q-axis equivalent magnetic circuit, reported in Fig. 3, can be solved to compute the no-load PM flux linkage and the q-axis inductance.

D. Iterative calculation of the q-axis inductance and PM flux

Based on the considerations reported in the previous subsections, the design of the PM dimension and the calculation of the q-axis quantities require an iterative procedure. In fact, the iron rib dimensions (w_r^i) structurally depend on the PM width w_{PM}^i (via the mass m_{PM}^i in eq. (20)), which in turn is electromagnetically affected by the iron ribs width as shown in eq. (27). The last equation also proves that the PM dimension is affected by the electromagnetic working point of the respective rib, i.e. from the two parameters B_{rib0}^i and $\mu_{rib-diff}^i$ included in R_{eq}^i. The latter follows from the resolution of the equivalent circuit which clearly depends also on the iron rib widths.

A comprehensive iterative procedure, summarized in the flowchart reported in Fig. 6, is here proposed to solve the non-linear q-axis magnetic circuit considering all the above mentioned dependencies between structural and electromagnetic design aspects. The SyRM design is a particular and simpler case of the PMaSyRM one. In particular, the workflow is constituted by the following steps.

1) For each machine defined by the two independent variables sr, mr, the design of the main stator and rotor dimensions is carried out (including the barrier height h_a^i and barrier surface S_b^i, tooth width w_t and tooth lenght l_t, and yoke length l_t) without considering the PM assistance as described in subsection II-A.
2) Then, the iron ribs dimension are calculated using eq. (20) without considering the PM weights and supposing a certain electromagnetic exploitation of the ribs, i.e. B_{rib}^i so

to be able to determine both B^i_{rib0} and $\mu^i_{rib-diff}$ needed to define their circuital representation.

3) Consequently, if a PMaSyRM is considered, the PM dimensions can be calculated (eq. 25-27) once the PM design criterion is selected. If the max ipf criterion is chosen, the q-axis inductance L_q required to evaluate λ^*_{PM-q} and so the PM widths w^*_{PM} is estimated at the first iteration using the approximate formulation reported in [21], [22] which does not require the resolution of the equivalent circuit. Otherwise (i.e SyRM case), the algorithm proceeds directly to step 5.
4) Once the PM widths are known, the iron ribs dimensions are re-calculated taking into account the PMs masses and compared with the previous values. If their difference lies within predefined bounds, the algorithm proceeds to the next step; otherwise, the PM widths are re-calculated considering the updated values of iron ribs w^i_r.
5) Once both PM and ribs dimensions are defined, the magnetic circuit is fully defined and it can be solved calculating the unknown rotor reaction $\Delta\mathbf{Z}$ via the eq. (23). The effective saturation level $B^i_{rib-new}$ in Fig. 5 can be evaluated for each iron rib with the following relationship:

$$B^i_{rib-new} = B^i_{rib0} + \frac{\Delta Z^i}{R^i_r} \cdot \frac{1}{w^i_r \cdot L} \tag{30}$$

The so computed value is then compared with the previous one (B^i_{rib}). If their difference is acceptable the algorithm proceeds to the next step; otherwise, the new value $B^i_{rib-new}$ is used to update the parameters of the tangent line (B^i_{rib0} and $\mu^i_{rib-diff}$) depicted in Fig. 5 and the algorithm restarts from the step 2 in the PMaSyRM case (re-calculating the PM dimensions) or step 5 in the SyRM case.
6) Once the saturation level of each rib is correctly evaluated, it is possible to fully define the variables related to the q-axis, i.e. the PM flux linkage and the q-axis inductance, considering either the PM or the stator excitation. If this calculation step is performed still modeling the iron ribs as the parallel between the flux generator ϕ^i_r and the reluctance R^i_r, then the rib working point (B^i_{rib}) would move on the line defined by the parameters ($B^i_{rib0-new}$ and $\mu^i_{rib-diff-new}$) depicted in Fig. 5. However, this approach would lead to incorrect estimation of λ_{PM} and L_q since the electromagnetic rib working points would differ from the load scenario (when both stator and PM excitations are present). To avoid this issue, the PM flux linkage and the q-axis inductance are calculated modeling the ribs with a single reluctance R^i_{r-app} defined by the apparent permeability ($\mu^i_{rib-app}$) as shown in Fig. 5:

$$R^i_{r-app} = \frac{h^i_r}{\mu^i_{rib-app} \cdot w^i_r \cdot L} \tag{31}$$

By doing so, the electromagnetic working points of all iron ribs are unequivocally fixed to the one related to the load scenario.

Therefore, the calculation of the q-axis inductance can be performed by modeling the iron ribs only with the apparent reluctances, turning off the PMs m.m.f. U^i_m and solving the resulting Thévenin magnetic circuit. Indeed, the resolution of such circuit leads to the calculation of the rotor magnetic potentials ΔZ^i. From these values it is possible to calculate the airgap flux ϕ^i_g flowing in each airgap branch of the magnetic circuit and, therefore, the airgap flux density B^i_g. Then, the complete waveform of B_g can be evaluated by combining all the calculated B^i_g (three in this case). From the obtained waveform, the first harmonic B_{g1} is calculated and used to compute the flux

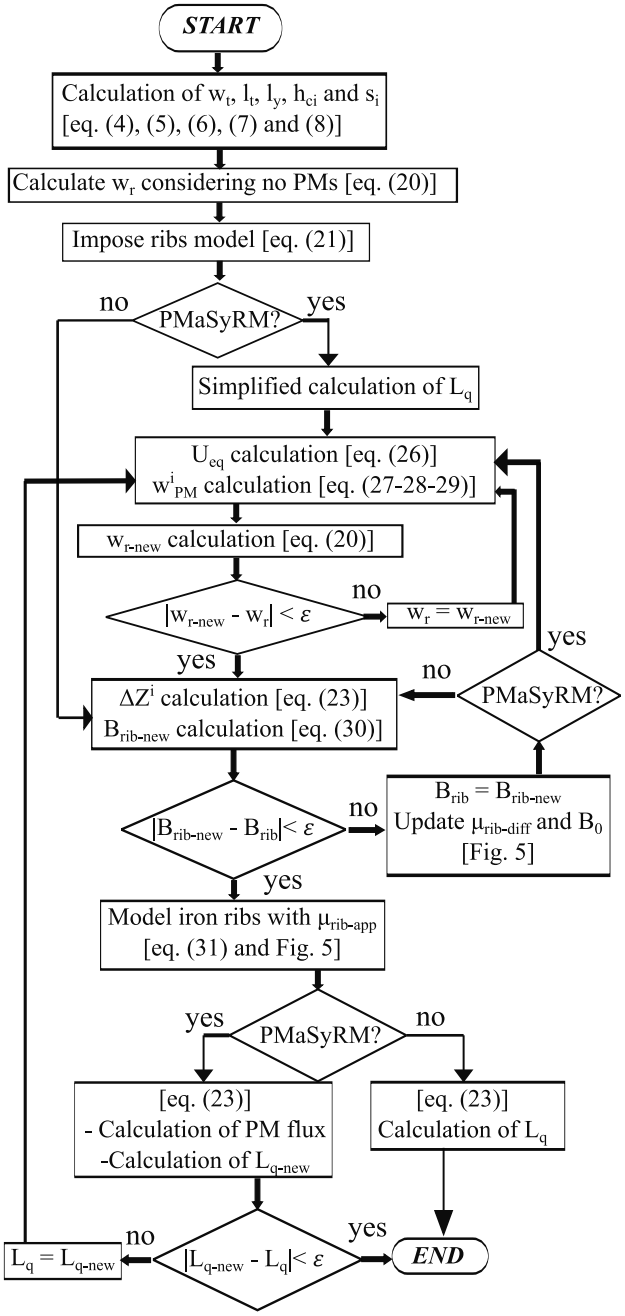

Fig. 6: Flowchart of the analytical design procedure.

per pole due to the q-axis current contribution and the inductance L_q as in (32):

$$L_q = \frac{2}{\pi} \cdot k_w \cdot N \cdot \tau_p \cdot L \cdot B_{g1} \tag{32}$$

where τ_p is the pole pitch in meters.

The same workflow can be adopted to calculate the flux per pole due to the PMs, by turning off the stator m.m.f. generators and applying the above procedure for the airgap flux density computation.

7) As last check and only for the PM-assisted machines, the computed L_q is compared with the one used to estimate the PM flux linkage needed to achieve the desired internal power factor (eq. (28)). If these two values are similar the algorithm ends, otherwise it restarts from step 2.

III. FE VALIDATION OF THE ANALYTICAL MODEL

The proposed analytical design approach has been implemented considering a wide range of design variables $sr - mr$. Table I summarizes the main assumptions and constraints. As previously pointed out, the outer envelope is fixed (i.e r_s and L are given).

The airgap thickness has been selected as a compromise choice between the need of mimizing it (beneficial from the electromagnetic point of view) and practical assembly limits, whereas the selected number of pole pairs allows a lower fundamental frequency beneficial for both control and thermal management. The stator and rotor materials are chosen so to minimize the iron losses and improve the rotor integrity at high-speed (further details about the materials selection can be found in [27]); the iron flux density is a consequence of the selected iron material for the stator lamination.

The PM dimensions have been designed to achieve an internal power factor ipf^* equal to 0.9. The estimated performance of each machine of the design plane $sr - mr$ has been compared with the respective FE analysis with the aim of investigating the accuracy of the analytical approach.

Fig. 7 reports a comparison between the analytical ($_{an}$) and FE computation ($_{FEA}$) of d-axis inductance (7a), q-axis inductance (7b) and PM flux linkage (7c). The empty areas of the design plane are due to the presence of unfeasible machines. The FE calculation of these three parameters have been performed with the frozen permeability method [28] in order to capture their values in the load scenario (i.e. when supplying with i_d, i_q and PM excitation). Analysing Fig. 7 it is worth to underline the good estimation of all parameters from a qualitative point of view. The excellent agreement of both q-axis inductance and PM flux linkage can be ascribed to the good estimation of the iron ribs saturation levels. Fig. 8 reports a comparison between the analytical and FE calculations of B_{rib} of each flux barrier. It is worth to notice that the contour plot of the outermost rib features an additional empty zone (left area of the design plane): the machine of such zone are still feasible but the respective outermost ribs width is zero or falls within the mechanical tolerance.

TABLE I: Design constraints and assumptions

Parameter	Value	Units
Outer stator radius	30	mm
Stack length	30	mm
Pole pairs	2	/
Airgap thickness	0.3	mm
N° of stator slots	24	/
N° of flux barriers per pole	3	/
Shape of flux barriers	U/I-shaped	/
Maximum speed	80000	rpm
Stator/rotor materials	JNHF600/35HXT780T	/
PM material	N42UH	/
Cooling capacity	30	kW/m^2
Iron flux density	1.4	T

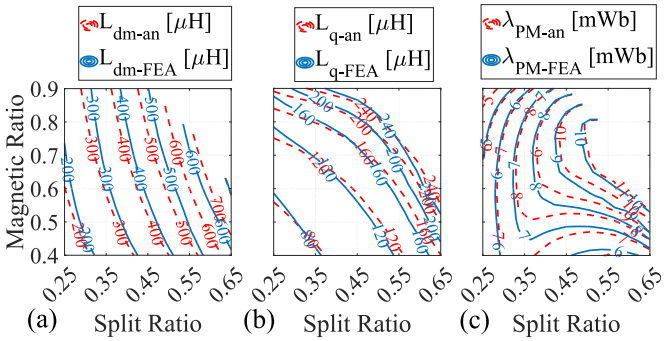

Fig. 7: Comparison between the analytical estimation and FE-computation of a) d-axis inductance, b) q-axis inductance and c) PM flux linkage at 80 krpm.

Although inductances and PM flux linkage are estimated with a good degree of accuracy, the torque, highlighted in Fig. 9a, shows non-negligible discrepancies respect to the FE-computed values. These residual errors are mainly due to the non-linear phenomena not considered in the analytical model, namely the cross-saturation effects (i.e L_{dq} and λ_{PM-d}).

Fig. 10a reports the percentage rate between the d- and q-axis PM flux linkage, whereas the influence of the cross-coupling contribution is shown in Fig. 10b in terms of percentage rate between L_{dq} and L_{dm}. The torque contour differs from the FE one mainly in the zone of the $sr - mr$ plane characterized by large cross-saturation phenomena. As a

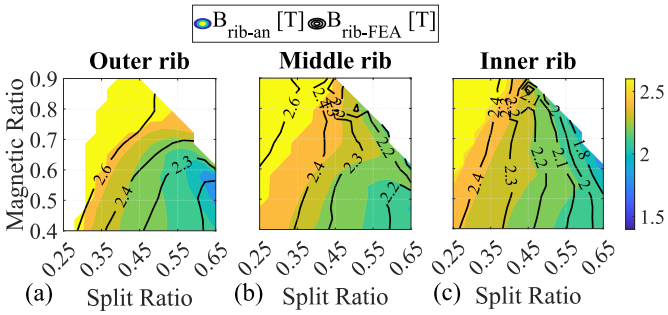

Fig. 8: Comparison between the analytical and FE calculations of B_{rib} of the a) outer barrier, b) middle barrier, c) inner barrier.

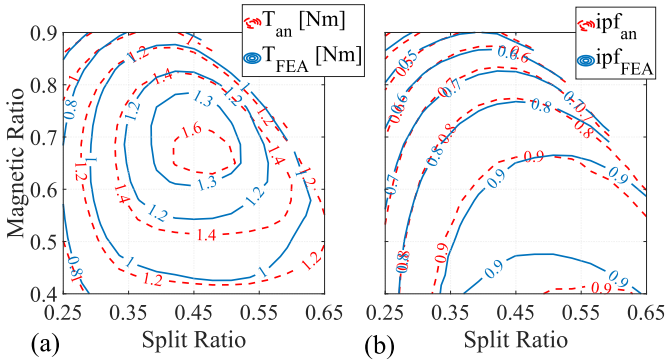

Fig. 9: Comparison between the analytical estimation and FE-computation of a) torque, b) ipf at 80krpm.

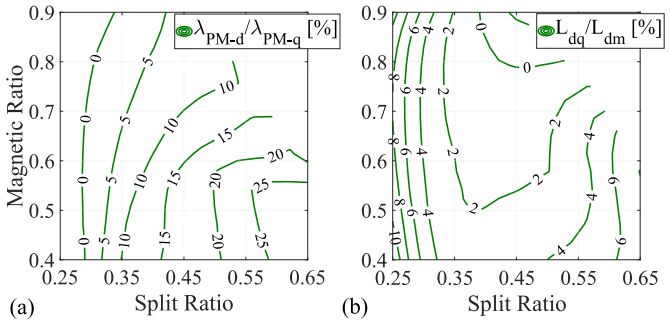

Fig. 10: Finite element computation of a) rate between the PM flux linkage along the d-axis and q-axis, b) rate between the cross-coupling inductance and the d-axis one.

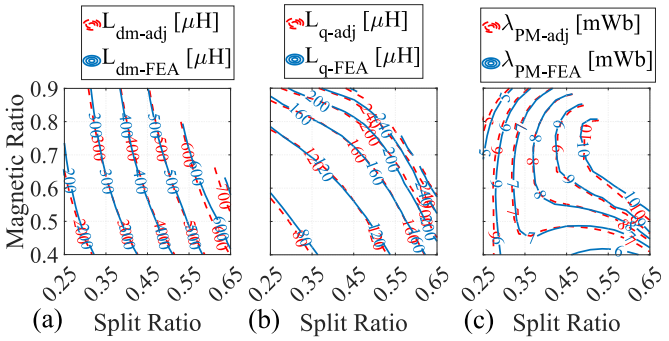

Fig. 11: Comparison between the adjusted estimation and FE-computation of a) d-axis inductance, b) q-axis inductance and c) PM flux linkage at 80 krpm.

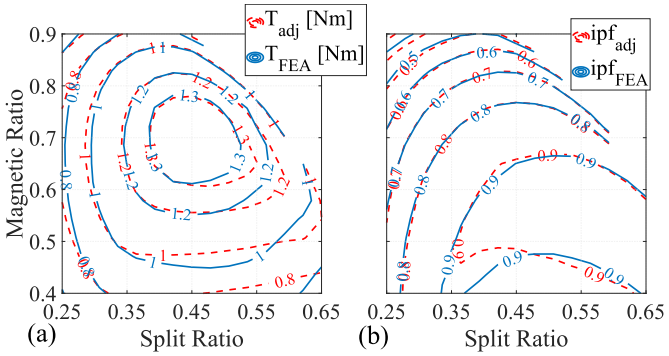

Fig. 12: Comparison between the adjusted estimation and FE-computation of a) Torque, b) ipf at 80 krpm.

consequence, the inclusion of such effects in the design stage is needed to reach an accurate prediction of the electromagnetic performance of both SyRM and PMaSyRM. Conversely, the analytical ipf contour shows a good agreement with the FE one, both in terms of numerical values and contour shape. It is worth to underline that the obtained internal power factor is not the desired one (i.e. 0.9) over the entire $sr-mr$ plane. In Section V the reason behind this behaviour will be fully investigated.

IV. Enhancing the Design Approach Accuracy

With the aim of improving the performance estimation without sacrificing the fast evaluation characteristic of the pure analytical approach, a hybrid design procedure, proposed in [20] for SyRMs, is extended here to the PM-assisted ones.

In particular, once the analytical design is performed for the whole $sr-mr$ plane, the 4 machines at the corners of the plane are selected and FE-simulated. From the FE-simulation all inductance (L_{dm}, L_{qm}, L_{dq} and L_s) and PM flux (λ_{PM-d} and λ_{PM-q}) contributions can be correctly evaluated adopting the frozen permeability method [28], [29]. This allows the calculation of several correction factors defined as the ratio between the finite element ($_{FEA}$) computed value and the respective analytical ($_{an}$) prediction as:

$$k_x^i = \frac{x_{FEA}^i}{x_{an}^i} \tag{33}$$

where x can be either the d- or q-axis PM flux linkage λ_{PM-d}, λ_{PM-q}, the magnetizing inductances L_{dm}, L_{qm}, the slot leakage inductance L_s or the cross coupling inductance L_{dq} of the i^{th} corner machine. The so computed correction factors are then extended to the entire design plane $sr-mr$ using a linear interpolation, allowing the adjustment of the magnetic model. By doing so, the cross-coupling terms (L_{dq} and λ_{PM-d}) are taken into account within the design workflow and the mismatches between analytical and FE-computed magnetizing inductances and q-axis PM flux are greatly reduced as shown in Fig. 11. The good agreement in terms of d- and q-axis inductances and PM flux linkage leads to the excellent matches between the adjusted torque and internal power factor contours shown in Fig. 12.

V. Preliminary Design Considerations

The reduction of the design space to only two variables (sr, mr) and the accurate calculation of torque and power factor as their function greatly reduce the design complexity. Indeed, the selection of the machine to be considered for the final design refinements (needed prior the prototyping) is greatly simplified. The choice of the final design is not univocal and clearly depends on the application requirements, e.g. the performance indexes having the priority (e.g. maximum torque, maximum power factor, minimum PM volume, etc.). In the following, the contours of the variables influencing mostly torque and power factor are analysed in order to infer the different trade-offs involved when designing high speed PMaSyR machines.

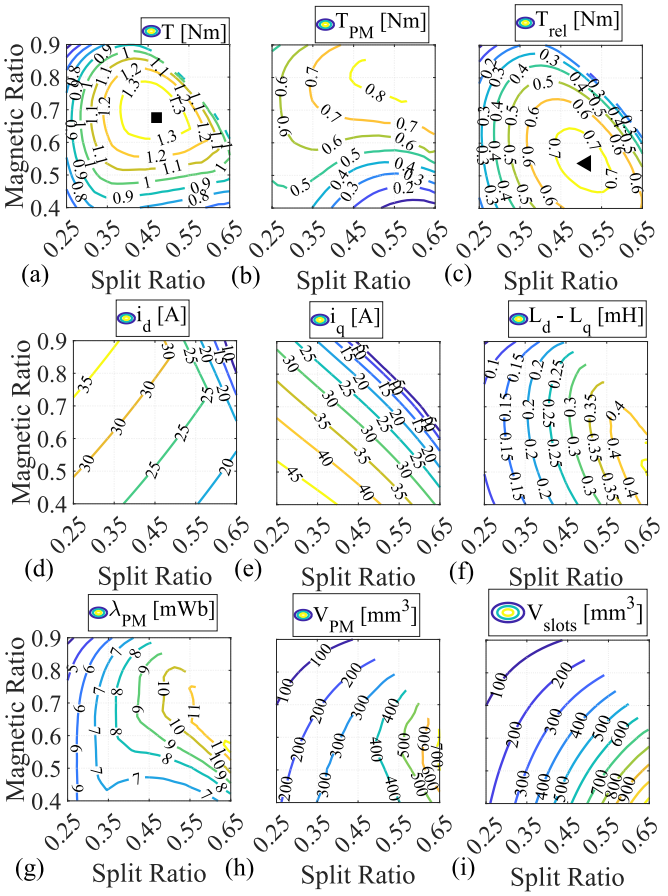

Fig. 13: Constant loci contour plot of a) total torque, b) PM torque, c) reluctance torque, d) i_d, e) i_q, f) $L_d - L_q$, g) PM flux, h) PM volume and i) Needed PM volume.

Fig. 13a, b and c report the constant loci in the $sr-mr$ plane of total torque, PM torque and reluctance torque component, respectively. The total torque contours and so the location of the maximum torque design (showed with the marker ■) depend on the concomitant actions of the reluctance and PM torques.

Fig. 13d, e and f show the contours of the variables defining the reluctance torque behaviour, namely the d- and q-axis currents and the inductances difference, respectively. It can be seen that the reluctance torque, and the location of the maximum reluctance torque design in the $sr-mr$ plane, is the compromise between the need of maximizing the magnetizing current (i_d), the anisotropy ($L_d - L_q$) and the quadrature current (i_q) [20], [22].

The shape of the PM torque component contours depends on both d-axis current (Fig. 13d) and PM flux linkage (Fig. 13g). The latter is heavily affected by the amount of PM material imposed by the selected PM design criterion, as it can be seen comparing subfigures 13g and 13h. The PM volume V_{PM} is also affected by the maximum available space within the rotor flux barriers (V_{slots}), shown in Fig. 13i.

Fig. 14a and 14b report the internal power factor of the PMaSyR machine and the respective value obtained without the PM assistance, respectively. Although the PM-assistance greatly improves the internal power factor respect to the pure

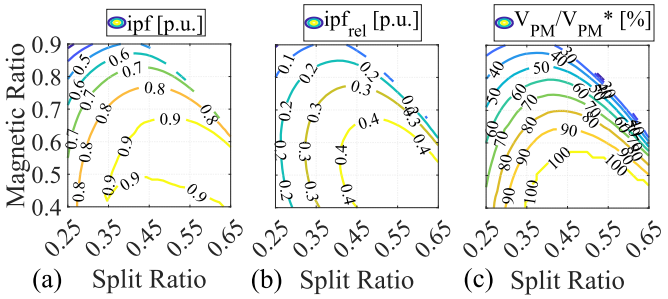

Fig. 14: Constant loci contour plot of a) ipf and b) ipf reluctance component and c) ratio between actual PM volume and needed one.

reluctance machines, only part of the design plane $sr - mr$ provides the target internal power factor (i.e. 0.9). For some region of the design plane, the PM volume required (V^*_{PM}) to satisfy the selected design criterion exceeds the available space within the rotor flux barriers. Fig. 14c reports the ratio between the effectively used PM volume and the ideally required value justifying this unexpected behaviour. In particular, the ipf values differ from the target one when designing machines with high magnetic ratio and low split ratio, as shown in Fig. 14a. Indeed, higher mr implies a higher thickness of the flux guides which reduces the flux barriers radial thickness (h^i) and so the available space for the PMs. Similarly, lower sr implies a reduction of the rotor diameter and so also of the flux barriers area.

Lastly, Fig. 15 shows the percentage difference between the module of the total flux and its d-axis components with respect to the latter. This figure of merit quantifies the approximation related to the assumption of neglecting the PM flux during the design of the stator tooth, yoke and rotor flux guides thicknesses. Analysing this figure, it is straightforward to conclude that the PM effect can be surely neglected during the magnetic design of the stator and rotor laminations. However, this does not imply that the PM presence should not influence the selection of the final machine. For example, selecting the design providing the maximum reluctance torque (shown with ▲ in Fig. 13c) and adding the PM within the rotor slots (according to a certain criterion) would lead to a sub-optimal design. In fact, the resulting machine would produce

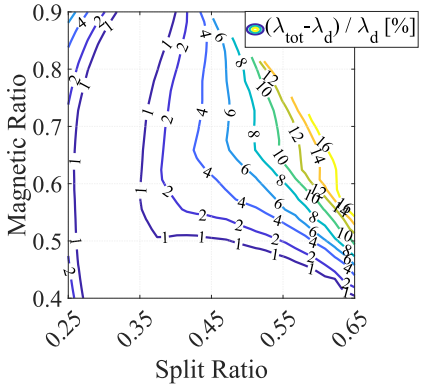

Fig. 15: Constant loci contour plot of the percentage difference between the module of the total flux and its d-axis components (in p.u. of the total flux).

a lower torque (1.1 Nm in this case) compared to the maximum torque design calculated considering both PM and reluctance components (1.4 Nm showed with ■ in Fig. 13a).

VI. Conclusion

This work has presented a general and comprehensive design procedure for high speed permanent magnet assisted synchronous reluctance machines. The proposed analytical design workflow allows considering all the non-linear aspects of the machine behaviour reducing to two the number of independent variables.

In particular, the resolution of the q-axis equivalent magnetic circuit has been proposed to calculate both q-axis inductance and PM flux linkage taking into account the non-linear behaviour of the rotor iron ribs. Then, an iterative procedure has been proposed to design the PM dimensions, to achieve a desired power factor, and to calculate the q-axis performance taking into account the electromagnetic non-linear behaviour of the iron ribs which are sized also considering the mechanical effect of the additional weight of the PMs. After FE validating the analytically predicted torque and power factor, a computational efficient FE-based approach has been implemented in order to enhance the accuracy of the analytical performance estimation.

The proposed hybrid analytical-FE design approach has been then applied to a specific case study to draw some preliminary design considerations. It has been shown how the PM-assistance can be neglected during the magnetic design of the stator and rotor laminations, and how this heavily affects the selection of the optimal machine.

In the next part of these two companion papers, the effects of the PM insertion when designing PMaSyRM with increasing maximum speed and different PM types will be analyzed in depth. Particular attention will be paid to the optimal machine selection and how this choice affects the maximum power capability and the overall geometry with respect to the operating speed. Then, all the FE refinements stages carried out before the manufacturing of the selected design will be shown along with the experimental test results.

References

[1] Nicola Bianchi, Emanuele Fornasiero, and Wen Soong. Selection of pm flux linkage for maximum low-speed torque rating in a pm-assisted synchronous reluctance machine. *IEEE Transactions on Industry Applications*, 51(5):3600–3608, 2015.

[2] Lei Hao, Chandra S. Namuduri, Suresh Gopalakrishnan, Chandra Mouli Mavuru, Prasad Atluri, and Thomas W. Nehl. Pm-assisted synchronous reluctance machine drive system for micro-hybrid application. *IEEE Transactions on Industry Applications*, 55(5):4790–4799, 2019.

[3] Gianmario Pellegrino, Alfredo Vagati, and Paolo Guglielmi. Design tradeoffs between constant power speed range, uncontrolled generator operation, and rated current of ipm motor drives. *IEEE Transactions on Industry Applications*, 47(5):1995–2003, 2011.

[4] Iman Kleilat, Khadija El Kadri Benkara, Guy Friedrich, Stéphane Vivier, Nazih Moubayed, and Rabih Dib. Comparison of two analytical methods for calculating the maximum mechanical stress in the rotor of high-speed-assisted synchronous reluctance machines. *IEEE Transactions on Industry Applications*, 57(2):1344–1353, 2021.

[5] Md. Zakirul Islam, Akm Arafat, Sai Sudheer Reddy Bonthu, and Seungdeog Choi. Design of a robust five-phase ferrite-assisted synchronous reluctance motor with low demagnetization and mechanical deformation. *IEEE Transactions on Energy Conversion*, 34(2):722–730, 2019.

[6] Chao Lu, Simone Ferrari, and Gianmario Pellegrino. Two design procedures for pm synchronous machines for electric powertrains. *IEEE Transactions on Transportation Electrification*, 3(1):98–107, 2017.

[7] Nicola Bianchi and Hanafy Mahmoud. An analytical approach to design the pm in pmarel motors robust toward the demagnetization. *IEEE Transactions on Energy Conversion*, 31(2):800–809, 2016.

[8] Yawei Wang, Giacomo Bacco, and Nicola Bianchi. Geometry analysis and optimization of pm-assisted reluctance motors. *IEEE Transactions on Industry Applications*, 53(5):4338–4347, 2017.

[9] Thanh Anh Huynh and Min-Fu Hsieh. Comparative study of pm-assisted synrm and ipmsm on constant power speed range for ev applications. *IEEE Transactions on Magnetics*, 53(11):1–6, 2017.

[10] Massimo Barcaro, Nicola Bianchi, and Freddy Magnussen. Permanent-magnet optimization in permanent-magnet-assisted synchronous reluctance motor for a wide constant-power speed range. *IEEE Transactions on Industrial Electronics*, 59(6):2495–2502, 2012.

[11] A. Vagati, B. Boazzo, P. Guglielmi, and G. Pellegrino. Design of ferrite-assisted synchronous reluctance machines robust toward demagnetization. *IEEE Transactions on Industry Applications*, 50(3):1768–1779, 2014.

[12] Barbara Boazzo. *Reduced-cost Permanent Magnet motor drives: a comprehensive design procedure and a universal approach to the magnetic model identification and control*. PhD thesis, Politecnico di Torino, IT, 2014.

[13] Nicola Bianchi, Michele Degano, and Emanuele Fornasiero. Sensitivity analysis of torque ripple reduction of synchronous reluctance and interior pm motors. *IEEE Transactions on Industry Applications*, 51(1):187–195, 2015.

[14] A. Credo, G. Fabri, M. Villani, and M. Popescu. Adopting the topology optimization in the design of high-speed synchronous reluctance motors for electric vehicles. *IEEE Transactions on Industry Applications*, 56(5):5429–5438, 2020.

[15] Yi Wang, Dan M. Ionel, Minjie Jiang, and Steven J. Stretz. Establishing the relative merits of synchronous reluctance and pm-assisted technology through systematic design optimization. *IEEE Transactions on Industry Applications*, 52(4):2971–2978, 2016.

[16] M. Di Nardo, M. Galea, C. Gerada, M. Palmieri, and F. Cupertino. Multi-physics optimization strategies for high speed synchronous reluctance machines. In *2015 IEEE Energy Conversion Congress and Exposition (ECCE)*, pages 2813–2820, 2015.

[17] Mauro Di Nardo, Giovanni Lo Calzo, Michael Galea, and Chris Gerada. Design optimization of a high-speed synchronous reluctance machine. *IEEE Transactions on Industry Applications*, 54(1):233–243, 2018.

[18] Nicola Bianchi, Hanafy Mahmoud, and Silverio Bolognani. Fast synthesis of permanent magnet assisted synchronous reluctance motors. *IET Electric Power Applications*, 10(5):312–318, 2016.

[19] Hanafy Mahmoud, Nicola Bianchi, Giacomo Bacco, and Nicola Chiodetto. Nonlinear analytical computation of the magnetic field in reluctance synchronous machines. *IEEE Transactions on Industry Applications*, 53(6):5373–5382, 2017.

[20] G. Gallicchio, M. Di Nardo, M. Palmieri, A. Marfoli, M. Degano, C. Gerada, and F. Cupertino. High speed synchronous reluctance machines: Modeling, design and limits. *IEEE Transactions on Energy Conversion*, 37(1):585–597, 2022.

[21] S. Ferrari and G. Pellegrino. Feafix: Fea refinement of design equations for synchronous reluctance machines. *IEEE Transactions on Industry Applications*, 56(1):256–266, 2020.

[22] A. Vagati, G. Franceschini, I. Marongiu, and G.P. Troglia. Design criteria of high performance synchronous reluctance motors. In *Conference Record of the 1992 IEEE Industry Applications Society Annual Meeting*, pages 66–73 vol.1, 1992.

[23] Gianmario Pellegrino, Paolo Guglielmi, Alfredo Vagati, and Franco Villata. Core losses and torque ripple in ipm machines: Dedicated modeling and design tradeoff. *IEEE Transactions on Industry Applications*, 46(6):2381–2391, 2010.

[24] I Boldea. *The Induction Machine Handbook*. CRC press, 01 2002.

[25] M. Di Nardo, M. Galea, C. Gerada, M. Palmieri, F. Cupertino, and Salem Mebarki. Comparison of multi-physics optimization methods for high speed synchrnous reluctance machines. In *IECON 2015 - 41st Annual Conference of the IEEE Industrial Electronics Society*, pages 002771–002776, 2015.

[26] N. Bianchi, T.M. Jahns, and IEEE Industry Applications Society. *Design, Analysis, and Control of Interior PM Synchronous Machines: Presented at the IEEE Industry Applications Society Annual Meeting, Seattle, USA, October 3rd, 2004*. CLEUP, 2004.

[27] Mauro Di Nardo, Gianvito Gallicchio, Marco Palmieri, Alessandro Marfoli, Giovanni Lo Calzo, Michele Degano, Chris Gerada, and

Francesco Cupertino. High-speed synchronous reluctance machines: Materials selection and performance boundaries. *IEEE Transactions on Transportation Electrification*, 8(1):1228–1241, 2022.

[28] W. Q. Chu and Z. Q. Zhu. Average torque separation in permanent magnet synchronous machines using frozen permeability. *IEEE Transactions on Magnetics*, 49(3):1202–1210, 2013.

[29] J. A. Walker, D. G. Dorrell, and C. Cossar. Flux-linkage calculation in permanent-magnet motors using the frozen permeabilities method. *IEEE Transactions on Magnetics*, 41(10):3946–3948, 2005.

Gianvito Gallicchio received the B.Sc. (Hons.) and M.Sc. (Hons.) degrees in electrical engineering from the Politecnico di Bari, Bari, Italy, in 2016 and 2018, respectively. He is currently working toward the Ph.D. degree with the Electrical Machines and Drives Group, Politecnico di Bari, Bari, Italy.

His main research interests include the design and analysis of permanent magnet and synchronous reluctance machines for both traction and high-speed applications, as well as the analysis, modeling and optimization of magnetic couplings.

Mauro Di Nardo (M'18) received the M.Sc. (Hons.) degree in electrical engineering from the Polytechnic University of Bari, Italy, in 2012, and the Ph.D. degree in electrical machine design from the University of Nottingham, U.K., in 2017. From 2017 to 2019, he was Head with the AROL R&D Team within the Polytechnic University of Bari leading industrial projects on electrical drives design for mechatronics applications.

Since the 2019, he is with the Power Electronics and Machine Control Group of the University of Nottingham as Research Fellow working on wide variety of projects. His research interests include the analysis, modelling, and design optimizations of permanent magnet and synchronous reluctance machines for automotive, aerospace and household sectors, induction motor for industrial applications as well as niche machine topologies such as bearingless and hysteresis motor.

He has been serving as an Associate Editor for the Open Journal of Industry Applications since March 2021.

Marco Palmieri received the M.Sc. and Ph.D. degrees in electrical engineering from Politecnico di Bari, Bari, Italy, in 2011 and 2016, respectively. Since 2017 he has been with the Department of Electrical and Information Engineering, Politecnico di Bari, where he is currently a post-doc researcher.

From 2011 to 2015, he was with the Energy Factory Bari Research Team, working on high-speed electrical machines for aeronautical applications. In 2014 he joined the Power Electronics, Control, and Machines Research Group of the University of Nottingham, working on electrical machines for aeronautical applications. In 2019 he was visiting researcher with the Laboratory of Actuation Technology of the Saarland University. His research interests include the design of high-speed electrical machines by means of optimization algorithms and finite element analysis.

Dr. Palmieri co-received the Prize Paper Award from the IEEE Industrial Electronics Society Electrical Machines Committee in 2015.

Alessandro Marfoli received the M.Sc. in Electrical Engineering from the University of Pisa, Italy, in 2015 and the Ph.D. degree in electrical machine design from the University of Nottingham (UK) in 2020. He is currently a Research Fellow within the same institution working on wide variety of projects of high industrial and scientific impacts.

His main research interests involves the modelling, analysis and optimization of electrical machines including induction and synchronous machines also for bearingless applications.

Michele Degano (SM'21) received his Master's degree in Electrical Engineering from the University of Trieste, Italy, in 2011, and his Ph.D. degree in Industrial Engineering from the University of Padova, Italy, in 2015. Between 2014 and 2016, he was a postdoctoral researcher at The University of Nottingham, UK, where he joined the Power Electronics, Machines and Control (PEMC) Research Group. In 2016 he was appointed Assistant Professor in Advanced Electrical Machines, at The University of Nottingham, UK. He was promoted Associate Professor in 2020.

His main research focuses on electrical machines and drives for industrial, automotive, railway and aerospace applications, ranging from small to large power.

He is currently the PEMC Director of Industrial Liaison leading research projects for the development of hybrid electric aerospace platforms and electric transports.

Chris Gerada (SM'12) is an Associate Pro-Vice-Chancellor for Industrial Strategy and Impact and Professor of Electrical Machines. His principal research interest lies in electromagnetic energy conversion in electrical machines and drives, focusing mainly on transport electrification. He has secured over £20M of funding through major industrial, European and UK grants and authored more than 350 referred publications. He received the Ph.D. degree in numerical modelling of electrical machines from The University of Nottingham, Nottingham, U.K., in 2005. He subsequently worked as a Researcher with The University of Nottingham on high-performance electrical drives and on the design and modelling of electromagnetic actuators for aerospace applications. In 2008, he was appointed as a Lecturer in electrical machines; in 2011, as an Associate Professor; and in 2013, as a Professor at The University of Nottingham. He was awarded a Research Chair from the Royal Academy of Engineering in 2013.

Prof. Gerada served as an Associate Editor for the IEEE Transactions on Industry Applications and is the past Chair of the IEEE IES Electrical Machines Committee.

Francesco Cupertino (M'08–SM'12) received the Laurea and Ph.D. degrees in electrical engineering from the Politecnico di Bari, Bari, Italy, in 1997 and 2001, respectively. Since 2001, he has been with the Department of Electrical and Information Engineering, Politecnico di Bari, Bari, Italy, where he is currently a Full Professor of converters, electrical machines, and drives.

He is the Scientific Director of four public/private laboratories at Politecnico di Bari that enroll more than 50 researchers; the laboratory Energy Factory Bari, with GE AVIO, aimed at developing research projects in the fields of aerospace and energy; the More Electric Transportation laboratory, with CVIT SpA (BOSCH Group), aimed at developing technologies for sustainable mobility; Cyber Physical Systems AROL Bari, with AROL SpA, focused on closure systems for food and beverage; Innovation for Mills, with Casillo Group and Idea75, focused in the Industry4.0 applications for wheat processing. He has authored or coauthored more than 130 scientific papers on these topics. His research interests include the design of synchronous electrical machines, motion control of high performances electrical machines, applications of computational intelligence to control, and sensorless control of ac electric drives.

Dr. Cupertino was the recipient of two Best Paper Awards from the Electrical Machines Committee of the IEEE Industry Application Society and from the homonymous Committee of the IEEE Industrial Electronics Society, in 2015.

He is currently the rector of Politecnico di Bari.